RSC Advances

ROYAL SOCIETY OF CHEMISTRY

www.rsc.org/advances

Graphical Abstract

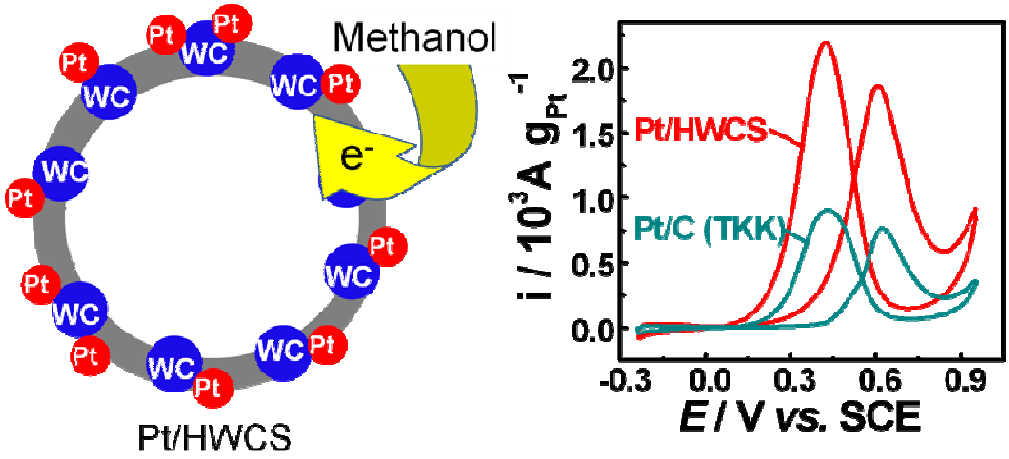

Hollow tungsten carbide/carbon sphere promoted Pt electrocatalyst for efficient methanol oxidation

Zaoxue Yan*, Fan Li, Jimin Xie*, Xuli Miu

School of Chemistry and Chemical Engineering, Jiangsu University, Zhenjiang, 212013, PR China;

*Corresponding authors. Tel.: +86 11 88791708; Fax: +86 11 88791800. E-mail: yanzaoxue@163.com (Z. Yan); xiejm391@sohu.com (J. Xie).

Abstract

The surface carbon thickness and particle size of tungsten carbide (WC) are critical to its synergistic effect on noble metal based electrocatalysts. We are demonstrating a synthesis of hollow tungsten carbide/carbon sphere composites (HWCSs) with thinner surface carbon and smaller particle size. The polystyrene sphere (PS) as template and P123 as surfactant favor dispersion of carbon and WC precursors, leading to HWCSs with smaller-sized WC and thinner surface carbon. The above factors in turn favor stable loading of smaller Pt particles on HWCSs, resulting in excellent electrocatalytic activity (due to synergistic effect) and stability (due to stronger interaction force between WC and Pt) of Pt/HWCS in electrocatalyzing methanol oxidation in acidic media. The present method is imagined to easily prepare other small-sized carbide particles with thinner surface carbon.

Keywords: Surface carbon; Tungsten carbide; Platinum electrocatalyst; Hollow sphere; Synergistic effect; Interaction force

1. Introduction

The commercialization of low temperature fuel cells depends on the reduction in cost.[1-5] To reduce the use amount of the noble metal based electrocatalyst[6,7] is an important resolution. It is reported that tungsten carbide (WC) has synergistic effect on noble metal based electrocatalysts both in anodic alcohol oxidation and cathodic oxygen reduction reaction.[8-15] The use level of noble metal can be significantly reduced to achieve the same or higher activity when WC is added. Literatures indicate that the synergistic effect between carbides and the noble metals increases with the decrease of carbide particle size[16,17] and surface carbon thickness[18]. However, the WC particles reported before were large or were coated by thick surface carbon,[19-22] resulting in low specific surface area and inferior contact with the loaded noble metals.

Many efforts have been made to obtain small-sized WC and other early transition metal carbide particles.[23-30] Cui et al. prepared WC nanoparticles with the diameter of 15 nm by in-situ carbonization with mesoporous silica as template, in which the template was used to hamper the conglomeration of WC.[31] Lu et al. prepared WC particles also with the diameter about 15 nm by a microwave heating method which avoided growth of WC particle.[32] Liang et al. reduced the WC size to 2-5 nm in diameter on carbon nanotubes with tungsten hexacarbonyl as tungsten precursor.[33] Recently, Fu's and Shen's groups reported a novel synthesis of carbides with the

diameter down to 2-10 nm through ion-exchange method.[34-37] A new formation mechanism of pure-phase WC that was transformed directly from $FeWO_4$ at low temperature under 600 ^oC was also put forward.[38] However, although small-sized WC particles have been obtained by various methods, most of the WC were wrapped by the large blocks of carbon or graphite substrate,[39-42] reducing contact with the loaded metals.

Herein, we report hollow tungsten carbide/carbon sphere composites (HWCSs) with hollow structure, small size of WC and thin surface carbon, which lead to more close contact and stronger interaction force between WC and the loaded Pt particles. Therefore, not only excellent catalytic activity (synergistic effect) but also excellent stability (stronger interaction force) was obtained towards methanol electro-oxidation (MOR).

2. Experimental

2.1 Preparation of the HWCS-1

Typically, 1.0 g polystyrene spheres (denoted as PSs), 2.0 g glucose, 1.8 g ammonium metatungstate (AMT, $(NH_4)_6W_7O_{24}.6H_2O$, A.R.) and some poly (ethylene glycol)-block-poly(propylene glycol)-block-poly(ethylene glycol) (denoted as P123) were impregnated in 40 ml of deionized water. The mixture was heated in a 50 ml autoclave at 180 ^oC for 12 h. Then the precipitate was washed with ethanol solution and dried at 90 ^oC. Afterwards, the dried product was heated in a microwave oven

(1000 W) for 160 s to remove the PSs. The product was then heated at 1000 ^{o}C for 7 h at nitrogen atmosphere and treated in 1.0 mol L^{-1} HCl solution to remove a little W_2C, and we got the final HWCS-1 composite. The "-1" in "HWCS-1" means 1 g PSs were used in the experimental process. P123 as long-chain dispersant is often used to synthesize porous substances,[43,44] and is used to disperse WC precursors in the present work. The P123 with masses of 0.00, 0.01, 0.03, 0.06 and 0.22 g in the HWCS-1 composites correspond to P123 content of 0.0 wt%, 0.5 wt%, 1.5 wt%, 3.0 wt% and 10.0 wt%, respectively, based on all the carbon sources.

2.2 Preparation of the HWCS-2

The preparation of HWCS-2 is similar to the preparation of HWCS-1. The difference is that 2 g of PSs and 1.5 wt% of P123 were added. The "-2" in "HWCS-2" means 2 g PSs were used in the preparation process.

2.3 Preparation of HCS-1 (hollow carbon spheres)

The preparation of HCS-1 is similar to the preparation of HWCS-1. The difference is that 1 g of PSs, 1.5 wt% of P123 and no AMT were added. The "-1" in "HCS-1" also means 1 g PSs were used in the preparation process.

2.4 Preparation of Pt electrocatalysts

Pt supported on the HWCS-1 (denoted as Pt/HWCS-1), HWCS-2 (denoted as Pt/HWCS-2) or HCS-1 (denoted as Pt/HCS-1) was prepared. Typically, HWCS-1, HWCS-2 or HCS-1 (50 mg) was added to a mixture of H_2PtCl_6 (containing 50 mg Pt) and 20 ml glycol and dispersed to uniform ink in ultrasonic bath for 30 min, the pH of the mixture was adjusted to 10 by 2 mol L^{-1} NaOH/glycol solution and put into a

microwave oven (900 W) for heating at a 12 s on and 12 s off procedure for 7 times. Afterward, the mixture was washed with deionized water and dried in vacuum at 60 ^{o}C for 4 h. The Pt content in the resulting product was targeted at 50 wt%.

2.5 Preparation of electrodes

4 mg of Pt/HWCS-1, Pt/HWCS-2, Pt/HCS-1 or commercial Pt/C (TKK, Japan) was dispersed in 1.95 ml ethanol and 0.05 ml 5 wt% Nafion suspension (DuPont, USA) under ultrasonic agitation to form the electrocatalyst ink. The electrocatalyst ink (0.005 ml) was deposited on a glassy carbon rod (0.25 cm^2) and dried at room temperature. The total Pt loadings were controlled at 0.02 mg cm^{-2}.

2.6 Electrochemical characterization

The electrochemical measurements were performed in a three-electrode cell on a potentiostat at 30 ^{o}C with the mixed solution of 0.5 mol L^{-1} H_2SO_4 and 1.0 mol L^{-1} methanol solution as electrolyte. A platinum foil (1.0 cm^2) and saturated calomel electrode (SCE) were used as counter and reference electrodes, respectively. Prior to electrochemical measurements, the electrolytic solution was purged with high-purity N_2 for 30 min to remove the dissolved oxygen.

2.7 Physical characterization

The morphologies of the synthesized materials were characterized by transmission electron microscopy (TEM, JOEP JEM-2010, JEOL Ltd.) operating at 200 kV, and thermal field emission environmental SEM-EDS-EBSD (Quanta 400F, FEI/OXFORD/HKL, Czech/France). The surface and pore structure were determined on a Physical Adsorption Instrument (ASAP 2400, Micrometeritics Co., USA). The

crystal structures were determined on an Xray diffractometer (XRD, D/Max-IIIA, Rigaku Co., Japan, CuK1, λ = 1.54056Å radiation).

3. Results and discussion

Figure 1a shows XRD patterns of the HWCS-1 (before HCl treatment) with P123 content of 0.0 wt%, 0.5 wt%, 1.5 wt%, 3.0 wt% and 10.0 wt%, respectively. The diffraction peaks at 2θ of 31.5°, 35.6° and 48.3° correspond to the (001), (100) and (101) facets of WC crystal by comparing JCPDS cards. And the diffraction peaks at 2θ of 34.5°, 38.0°, 39.6° and 52.3° correspond to the (100), (002), (101) and (102) facets of W_2C crystal. The WC (101) peak can be used to calculate the crystal size according to the Scherrer's equation (1)

$$D = K\lambda/(B\cos\theta) \quad (1)$$

where D denotes the average diameter in nm, K the Scherrer constant (0.89), λ the wavelength of X-ray (λ=0.154056 nm), B the corresponding full width at half maximum (FWHM) and θ the Bragg's diffraction angle. Figure 1b summarizes the relation between the calculated WC crystal size and the P123 mass content, which shows the WC crystal size decreasing with the increase of P123 mass content. Furthermore, it can be seen from Figure 1a that the WC intensity increases and the W_2C intensity decreases with the increase of P123 mass content. The reasons are as follows. As was reported, W precursor can be carburized to W_2C, then to WC;[45] the smaller particles of W precursor (correspond to more P123 mass ratio) are easier to be

carburized to WC due to shorter carburization path. Among the five samples in Figure 1, P123 at the content of 1.5 wt% makes the relatively small WC crystal size (14.6 nm) and high WC intensity. So the HWCS-1 with 1.5 wt%-P123 was focused on for further studies.

Figure 2a is the SEM image of HWCS-1 before HCl treatment, which shows white dots uniformly dispersed on black spheres. Figure 2b is its TEM image, which shows uniform black dots. These white and black dots are determined as nearly pure WC by XRD result (Figure 1). From the WC particle size distribution (Figure 2e) randomly measured from 100 particles (Figure 2b), the average diameter of WC in HWCS-1 is calculated as 14.3 nm, being consistent with the XRD result (14.6 nm). For comparison, the morphology of HWCS without P123 before HCl treatment was also characterized, and its SEM and TEM images are showed in Figure 2c and its inset. From the images, serious conglomerations of white or black dots are observed, and the average diameter of the dots is calculated as 24.0 nm (see Figure 2f). However, the XRD result (Figure 1) shows the dots being dominantly W_2C. The above results confirm that the larger precursor particles are difficult to be transformed to WC.

The effect of PS amount on the size of WC and surface carbon thickness was also studied. Typically, we doubled the PS amount in the preparation process and got HWCS-2, whose TEM image is shown in Figure 2d. Obviously, the carbon thickness[46] in HWCS-2 is less than that in HWCS-1, in other words, the WC in HWCS-2 has more exposure. The WC particle size distribution in HWCS-2 is shown in Figure 2g, and the corresponding WC average particle size is calculated as 13.4 nm,

being slightly smaller than that in HWCS-1. It seems that the WC particle size is restricted by the carbon layer thickness.

The HWCS-1 and HWCS-2 were further characterized by BET analysis. Figure S1 shows the N_2 adsorption-desorption isotherms and pore size distributions. Table 1 summarizes the surface areas, pore volumes and average pore diameters. It shows that the HWCS-1 has a total surface area of 433 $m^2 g^{-1}$, total pore volume of 0.25 $cm^3 g^{-1}$ and an average pore diameter of 0.46 nm, and the HWCS-2 has a total surface area of 738 $m^2 g^{-1}$, total pore volume of 0.46 $cm^3 g^{-1}$ and an average pore diameter of 0.49 nm. Obviously, the HWCS-2 has improved surface structure than HWCS-1.

The higher surface area, more exposure (or thinner surface carbon) and smaller-sized WC of HWCSs are expected to give Pt/HWCSs better performances. Pt particles were loaeded on the HWCS-1, HWCS-2 and HCS-1 to form electrocatalysts. Figure 3 shows the XRD patterns of the three electrocatalysts. The peaks at 39.8°, 46.2° and 67.5° correspond to the (111), (200) and (220) facets of Pt crystal by comparing JCPDS cards. According to Scherrer's equation (1), the Pt particle size in Pt/HCS-1 is calculated as 3.6 nm. The Pt particle size in Pt/HWCS-1 and Pt/HWCS-2 cannot be accurately calculated because the Pt peaks are overlapped with the WC peaks. However, the FWHMs of Pt peaks on Pt/HWCS-1 and Pt/HWCS-2 are obviously wider than that on Pt/HCS-1, indicating the smaller Pt sizes in Pt/HWCS-1 and Pt/HWCS-2. Reports indicate that stronger interaction force existes between carbides and noble meatals,[47,48] which should account for the loading of smaller Pt particles on HWCSs.

Figure 4a is the TEM image of Pt/HWCS-1, no conglomeration can be seen. Figure 4b and 4c show the Pt and WC crystal lattices in Pt/HWCS-1. Figure 4d shows sparser and smaller WC and Pt particles in Pt/HWCS-2. Figure 4e shows obviously conglomerated Pt particles in Pt/HCS-1. All the WC and Pt particle sizes showed in Figure 4 are consistent with the TEM and XRD results (Figure 2 and 3). In addition, the EDS patterns (inset of Figure 4a and 4d) for Pt/HWCS-1 and Pt/HWCS-2 confirm the coexistence of Pt, C and W elements (the peaks of Cu and Cr elements come from sample bracket).

The improvement in MOR is significant for improving the performance of proton exchange membrane fuel cells. Figure 5a shows the cyclic voltammograms of MOR on Pt/HWCS-1, Pt/HWCS-2, Pt/HCS-1 and Pt/C (TKK) electrodes. The peak current density and onset potential for each electrocatalyst are listed in Table 2. In the following sections, we will firstly compare the performances of Pt/HWCS-1, Pt/HCS-1 and Pt/C, then compare that of Pt/HWCS-1 and Pt/HWCS-2.

Firstly it can be seen that the Pt/HCS-1 has slightly higher performance than the Pt/C (TKK), which should result from the high specific surface area of HCS-1. It also can be seen that the Pt/HWCS-1 has much higher performance than the Pt/HCS-1, it should result from the addition of WC. As to the higher performance of Pt/HWCS-1 than that of Pt/C (TKK), it should be due to both the high specific surface area of HWCS-1 and the existence of WC in Pt/HWCS-1. It is noteworthy that the peak current density on Pt/HWCS-1 (1517 mA mg_{Pt}^{-1}) is 1.96 times that on Pt/C (TKK) (773 mA mg_{Pt}^{-1}), and the onset potential for MOR on Pt/HWCS-1 is negatively

shifted about 150 mV. This is a significant improvement since a direct methanol fuel cell gives only less than 0.5 V output voltage at reasonable current density, leading to an expected 30% improvement in electric efficiency.

The electrochemical active surface areas (EASAs) can be used to analyze the performances of the synthesized materials. Figure 5b shows the cyclic voltammograms of the four electrodes in 0.5 mol L^{-1} H_2SO_4 solution. Their EASAs can be calculated according to the following equation (2):[48]

$$EASA = \frac{Q}{Q_H} = \frac{1}{Q_H}[\frac{1000}{a_0 v_0} \times \int_{E_1}^{E_2} (I - I_0) d(E - E_1)] \qquad (2)$$

where I is the current density (mA cm^{-2}), E the potential (V); I_0, E_1 and E_2 are the current density and potentials at the initial and terminal points of hydrogen desorption peak; a_o is the Pt loading normalized to the electrode surface area (mg_{Pt} cm^{-2}), v_o the scan rate (mV s^{-1}), Q_H the hydrogen adsorption electric quantity for a smooth polycrystalline Pt (Q_H =2.10 C m^{-2}), and Q is the electric quantity in the hydrogen desorption peak and normalized to Pt loadings (C g_{Pt}^{-1}). According to equation (2), the EASAs for the electrodes were calculated and also listed in Table 2. It can also be calculated that the ratios of EASAs on Pt/HWCS-1 and Pt/C (TKK) are 1.60: 1, which are obviously smaller than the corresponding ratios of peak current densities (1.96: 1). That is to say, the EASA is not the sole factor to determine the performances of electrocatalysts, there should exist synergistic effect as mentioned above to further promote the catalytic activity of Pt/HWCS-1.

Secondly, we compared the electrocatalysts of Pt/HWCS-1 and P/HWCS-2 (Figure

5). The Pt/HWCS-2 has the peak current density of 1860 mA mg_{Pt}^{-1}, which is 1.23 times that of Pt/HWCS-1. And the EASA of Pt/HWCS-2 (82.9 m2 g-1) is 1.15 times that of Pt/HWCS-1. Moerover, the Pt/HWCS-2 has more negative onset potential than Pt/HWCS-1. The results indicate that the HWCS-2 with more exporsure of WC has more promotion effect on Pt than that of HWCS-1 .

The stabilities of the Pt/HWCS-1, Pt/HWCS-2 and Pt/C (TKK) electrodes for MOR are shown in Figure 5c and 5d. The shadows are the cycling difference between the 1st cycle and the 5,000th cycle. It can be seen that the activity of the commercial Pt/C (TKK) reduced 21.7% from 767.8 mA mg_{Pt}^{-1} to 601.1 mA mg_{Pt}^{-1} by comparing the peak current density. The activity of the Pt/HWCS-1 reduced 6.7% from 1517 mA mg_{Pt}^{-1} to 1416 mA mg_{Pt}^{-1}. And the activity of the Pt/HWCS-2 reduced 5.1% from 1860 mA mg_{Pt}^{-1} to 1766 mA mg_{Pt}^{-1}. The results indicate that WC supported electrocatalysts are more stable than the sole carbon supported electrocatalyst, and the WC with more exposure leads to higher stability of Pt loaded electrocatalyst.

The excellent activity and stability of Pt/HWCSs are explained by synergistic effect and strong interaction force between the WC support and the active Pt metal. Literatures reported that synergistic effect exists between carbides and noble metals caused by electron transfer between them.[48-50] The surface electronic structure of Pt/WC was therefore very different from that of Pt/C, and showed an obvious anti-CO-poisoning effect in the electrooxidation of methanol. This may be the origin of the excellent activity of the Pt/HWCSs. On the other hand, the electron transfer between WC and Pt means a high linkage (strong interaction force) between them,

which account for the excellent electrocatalytic stability of Pt/HWCS. Moreover, the more exposure of WC lead to more close contact with the loaded Pt particles, then higher activity and stability can be consequently obtained.

4. Conclusions

HWCSs with more exposure (or thinner surface carbon) and smaller WC particle size were synthesized. The thickness of surface carbon around WC can be reduced by improving the ratio of PS to glucose. The WC particle size can be reduced by both increasing the amount of P123 as dispersant and improving the ratio of PS to glucose. The smaller-sized WC particles with more exposure lead to stable loading of smaller-sized Pt particles and close contact between them, which not only show excellent activity for catalyzing MOR due to synergistic effect, but also show more stability due to stronger interaction force. The present work is imagined to be easily used to prepare other small-sized particles with thin surface carbon.

Acknowledgements

This work was financially supported by China Postdoctoral Science Foundation (2014T70481), National Natural Science Foundation of China (21306067), Natural Science Foundation of Jiangsu (BK20130490), College Natural Science Research Program of Jiangsu Province (12KJB150007) and China Postdoctoral Science

Foundation (2013M541609). Jimin Xie thanks the Industry High Technology Foundation of Jiangsu (BE2013090).

References

1 Y. Dong, H. Pang, H. Yang, J. Jiang, Y. Chi and T. Yu, *RSC Adv.*, 2014, **4**, 32791-32795.

2 C. W. Liu, C. M. Lai, J. N. Lin, L. D. Tsai and K. W. Wang, *RSC Adv.*, 2014, **4**, 15820-15824.

3 Y. Zhou, X. Hu, Y. Xiao and Q. Shu, *Electrochim. Acta*, 2013, **111**, 588-592.

4 Y. Bing, H. Liu, L. Zhang, D. Ghosh and J. Zhang, *Chem. Soc. Rev.*, 2010, **39**, 2184-2202.

5 Q. Wang, X. Wang, Z. Chai and W. Hu, *Chem. Soc. Rev.*, 2013, **42**, 8821-8834.

6 M. K. Jeona, K. R. Leea, W. S. Leea, H. Daimonb, A. Nakaharab, S. I. Woo, *J. Power Sources*, 2008, **185**, 927-931.

7 M. Liu, R. Zhang and W. Chen, *Chem. Rev.,* 2014, **114**, 5117-5160.

8 Y. W. Lee, A. R. Ko, D. Y. Kim, S. B. Han and K. W. Park, *RSC Adv.*, 2012, **2**, 1119-1125.

9 M. D. Obradović, B. M. Babić, V. R. Radmilović, N. V. Krstajić and S. L. Gojković, *Int. J. Hydrogen Energy*, 2012, **37**, 10671-10679.

10 K. Wang, Y. Wang, Z. Liang, Y. Liang, D. Wu, S. Song and P. Tsiakaras, *Appl. Catal. B-Environ.*, 2014, **147**, 518-525.

11 M. Rahsepar, M. Pakshir, P. Nikolaev, A. Safavi, K. Palanisamy and H. Kim, *Appl. Catal. B-Environ.*, 2012, **127**, 265-272.

12 N. R. Elezović, B. M. Babić, L. Gajić-Krstajić, P. Ercius, V. R. Radmilović, N. V. Krstajić and L. M. Vračar, *Electrochim. Acta*, 2012, **69**, 239-246.

13 Z. Y. Chen, C. A. Ma, Y. Q. Chu, J. M. Jin, X. Lin, C. Hardacre and W. F. Lin, *Chem. Commun.*, 2013, **49**, 11677-11679.

14 C. Ma, L. Kang, M. Shi, X. Lang and Y. Jiang, *J. Alloy. Compd.*, 2014, **588**, 481-487.

15 T. G. Kelly and J. G. Chen, *Chem. Soc. Rev.*, 2012, **41**, 8021-8034.

16 Z. Yan, H. Meng, P. K. Shen, R. Wang, L. Wang, K. Shi and H. Fu, *J. Mater. Chem.*, 2012, **22**, 5072-5079.

17 Z. Yan, H. Wang, M. Zhang, Z. Jiang, T. Jiang and J. Xie, *Electrochim. Acta*, 2013, **95**, 218-224.

18 D. V. Esposito, S. T. Hunt, Y. C. Kimmel and J. G. Chen, *J. Am. Chem. Soc.*, 2012, **134**, 3025–3033.

19 Y. Wang, S. Song, V. Maragou, P. K. Shen and P. Tsiakaras, *Appl. Catal. B-Environ.*, 2009, **89**, 223-228.

20 C. Ma, L. Kang, M. Shi, X. Lang and Y. Jiang, *J. Alloy Compd.*, 2014, **588**, 481-487.

21 H. Singh and O. P. Pandeyn, *Ceram. Int.*, 2013, **39**, 6703-6706.

22 P. K. Shen, S. Yin, Z. Li and C. Chen, *Electrochim. Acta,* 2010, **55**, 7969-7974.

23 S. Yin, M. Cai, C. Wang and P. K. Shen, *Energ. Environ. Sci.*, 2011, **4**, 558-563.

24 Y. Liu and W. E. Mustain, *ACS Catal.*, 2011, **1**, 212-220.

25 Y. Yan, B. Xia, X. Qi, H. Wang, R. Xu, J. Y. Wang, H. Zhang and X. Wang,

Chem. Commun., 2013, **49**, 4884-4886.

26 X. Tao, Y. Li, J. Du, Y. Xia, Y. Yang, H. Huang, Y. Gan, W. Zhang and X. Li, *J. Mater. Chem.*, 2011, **21**, 9095-9102.

27 Q. Zhu, S. Zhou, X. Wang and S. Dai, *J. Power Sources*, 2009, **193**, 495-500.

28 A. T. Garcia-Esparza, D. Cha, Y. Ou, J. Kubota, K. Domen and K. Takanabe, *ChemSusChem*, 2013, **6**, 168-181.

29 F. Teng, J. Wang, X. An, B. Lu, Y. Su, C. Gong, P. Zhang, Z. Zhang and E. Xie, *RSC Adv.*, 2012, **2**, 7403-7405.

30 K. G. Nishanth, P. Sridhar, S. Pitchumani and A. K. Shukla, *Fuel Cell*, 2012, **12**, 146-152.

31 X. Cui, X. Zhou, H. Chen, Z. Hua, H. Wu, Q. He, L. Zhang and J. Shi, *Int. J. Hydrogen Energy*, 2011, **36**, 10513-10521.

32 J. L. Lu, Z. H. Li, S. P. Jiang, P. K. Shen and L. Li, *J. Power Sources*, 2012, **202**, 56-62.

33 C. Liang, L. Ding, A. Wang, Z. Ma, J. Qiu and T. Zhang, *Ind. Eng. Chem. Res.*, 2009, **48**, 3244-3248.

34 R. Wang, C. Tian, L. Wang, B. Wang, H. Zhang and H. Fu, *Chem. Commun.*, 2009, 3104-3106.

35 G. He, Z. Yan, M. Cai, P. K. Shen, M. R. Gao, H. B. Yao and S. H. Yu, *Chem.-Eur. J.*, 2012, **18**, 8490-8497.

36 Z. Hu, Z. Yan, P. K. Shen and C. J. Zhong, *Nanotechnology*, 2012, **33**, 485404.

37 Z. Yan, M. Zhang, J. Xie and P. K. Shen, *J. Power Sources*, 2013, **243**, 336-342.

38 Z. Yan, M. Cai and P. K. Shen, *Sci. Rep.-UK*, 2013, **3**, 1646.

39 X. Yang, Y. C. Kimmel, J. Fu, B. E. Koel and J. G. Chen, *ACS Catal.*, 2012, **2**, 765-769.

40 Y. C. Kimmel, D. V. Esposito, R. W. Birkmire and J. G. Chen, *Int. J. Hydrogen Energy*, 2012, **37**, 3019-3024.

41 T. Ryu, H. Y. Sohn, K. S. Hwang and Z. Z. Fang, *J. Am. Ceram. Soc.,* 2009, **92**, 655-660.

42 S. Sharma and B. G. Pollet, *J. Power Sources*, 2012, **208**, 96-119.

43 Z. Fu, Q. M. Huang, X. D. Xiang, Y. L. Lin, W. Wu, S. J. Hu and W. S. Li*, Int. J. Hydrogen Energy*, 2012, **37**, 4704-4709.

44 M. Lei, T. Z. Yang, W. J. Wang, K. Huang, R. Zhang, X. L. Fu, H. J. Yang, Y. G. Wang and W. H. Tang, *Int. J. Hydrogen Energy*, 2013, **38**, 205-211.

45 Y. Wang, S. Song, P. K. Shen, C. X. Guo and C. M. Li, *J. Mater. Chem.,* 2009, **19**, 6149-6153.

46 Z. Yan, Z. Hu, C. Chen, H. Meng, P. K. Shen, H. Ji and Y. Meng, *J. Power Sources*, 2010, **195**, 7146-7151.

47 Z. Yan, J. Xie, P. K. Shen, M. Zhang, Y. Zhang and M. Chen, *Electrochim. Acta*, 2013, **108**, 644-650.

48 Z. Yan, G. He, P. K. Shen, Z. Luo, J. Xie and M. Chen, *J. Mater. Chem. A*, 2014, **2**, 4014-4022.

49 R. Wang, Y. Xie, K. Shi, J. Wang, C. Tian, P. Shen and H. Fu, *Chem.-Eur. J.*, 2012, **18**, 7443-7451.

50 G. Cui, P. K. Shen, H. Meng, J. Zhao and G. Wu, *J. Power Sources,* 2011, **196**, 6125−6130.

Table Captions

Table 1 Surface structure of HWCS-1 and HWCS-2

Table 2 The performance comparison of the four electrocatalysts

Figure Captions

Figure 1 (a) XRD patterns of HWCS-1 with different P123 mass content, (b) the effect of P123 mass content on crystal size of WC.

Figure 2 (a) SEM images of HWCS-1; (b) TEM image of HWCS-1; (c) SEM image of HWCS without P123, inset is the corresponding TEM image; (d) TEM image of HWCS-2; (e), (f) and (g) are the particle size distributions obtained from Figure 2b, inset in Figure 2c and Figure 2d, respectively.

Figure 3 XRD patterns of Pt/HWCS-1, Pt/HWCS-2 and Pt/HCS-1.

Figure 4 (a) TEM image of Pt/HWCS-1; (b, c) HRTEM images of Pt/HWCS-1; (d) TEM image of Pt/HWCS-2; (e) TEM image of Pt/HCS-1; insets of (a) and (d) are the corresponding EDS patterns of Pt/HWCS-1 and Pt/HWCS-2.

Figure 5 (a) Cyclic voltammograms of MOR on Pt/HWCS-1, Pt/HWCS-2, Pt/HCS-1 and Pt/C (TKK) electrodes in 0.5 mol L^{-1} H_2SO_4/1.0 mol L^{-1} methanol solution; (b) cyclic voltammograms on the four electrodes in 0.5 mol L^{-1} H_2SO_4 solution; (c) the cyclic voltammograms of MOR on Pt/HWCS-1, Pt/HWCS-2 and Pt/C (TKK) electrodes in 0.5 mol L^{-1} H_2SO_4/1.0 mol L^{-1}

methanol solution; (d) the cyclic voltammograms on the three electrodes in 0.5 mol L^{-1} H_2SO_4 solution. All the cyclic voltammogram experiments were carried out at 30 ^{o}C with the scan rate of 50 mV s^{-1}. And the shadows in (c) and (d) show the difference between the 1st cycle and the 5,000th cycle.

Table 1 Surface structure of HWCS-1 and HWCS-2

Sample	Total surface area / $m^2 g^{-1}$	Micropore area / $m^2 g^{-1}$	Total pore volume / $cm^3 g^{-1}$	Micropore volume / $cm^3 g^{-1}$	Average pore diameter/ nm
HWCS-1	433	361	0.25	0.17	0.46
HWCS-2	738	598	0.46	0.30	0.49

Table 2 The performance comparison of the four electrocatalysts

Electrocatalyst	Pt mass content*	Peak current density (mA mg_{Pt}^{-1})	Onset potential (V)	EASA (m^2 g^{-1})
Pt/HWCS-1	47.9 %	1517	0.25	71.9
Pt/HWCS-2	48.3%	1860	0.24	82.9
Pt/HCS-1	47. 1%	926	0.39	50.1
Pt/C (TKK)	47.6 %	773	0.40	44.9

* The data were determined by inductively coupled plasma-atomic emission spectrometry (ICP).

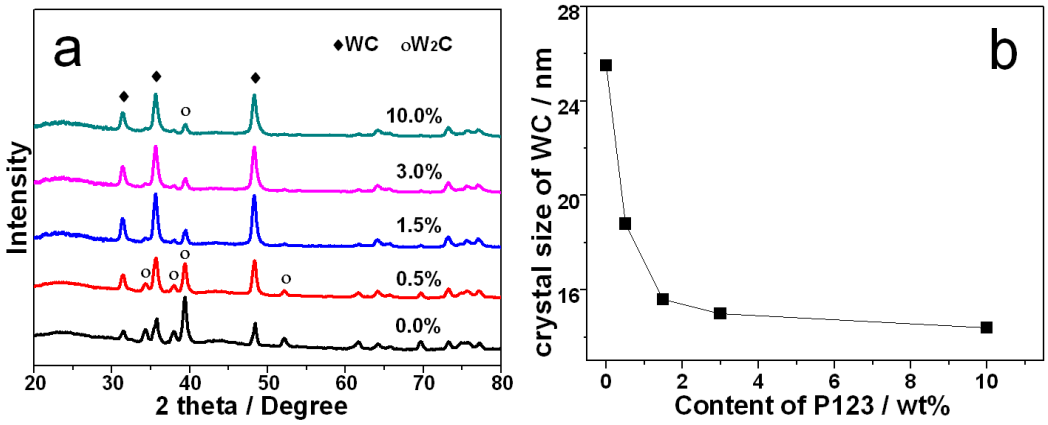

Figure 1

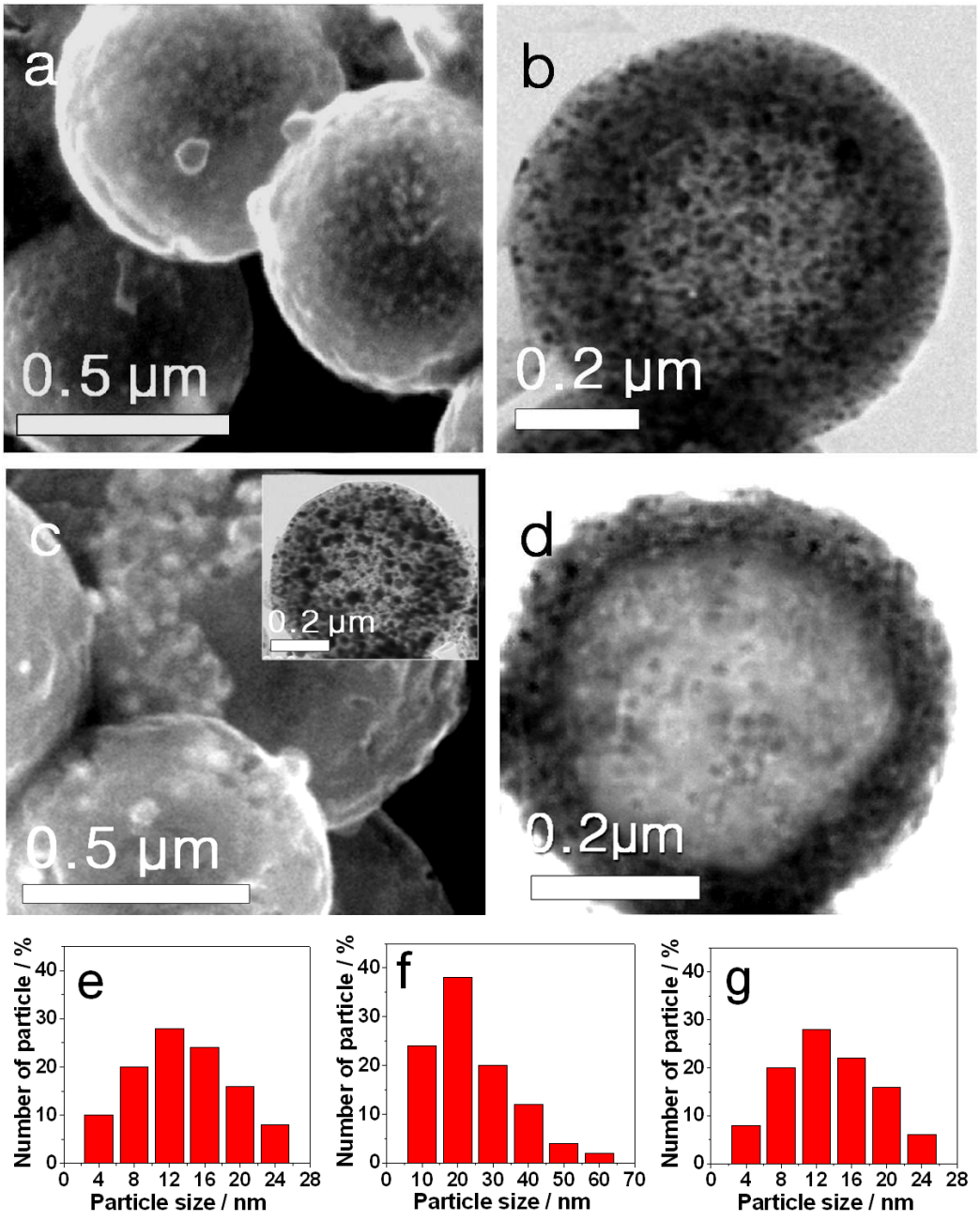

Figure 2

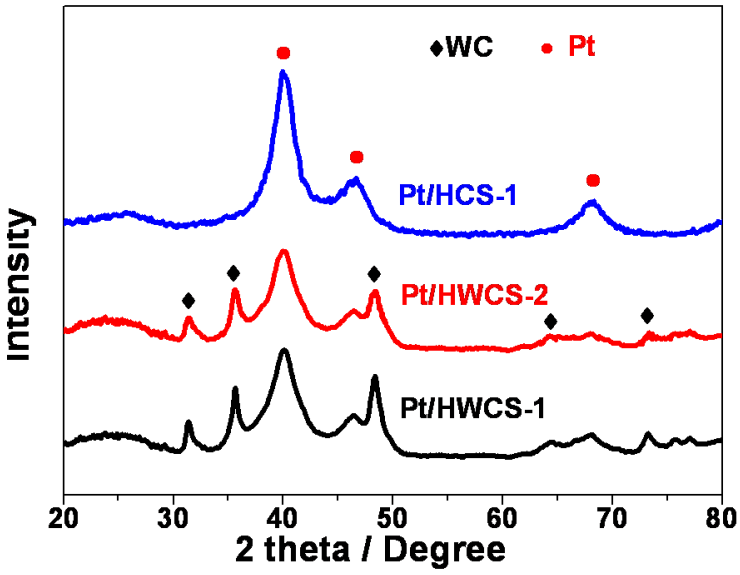

Figure 3

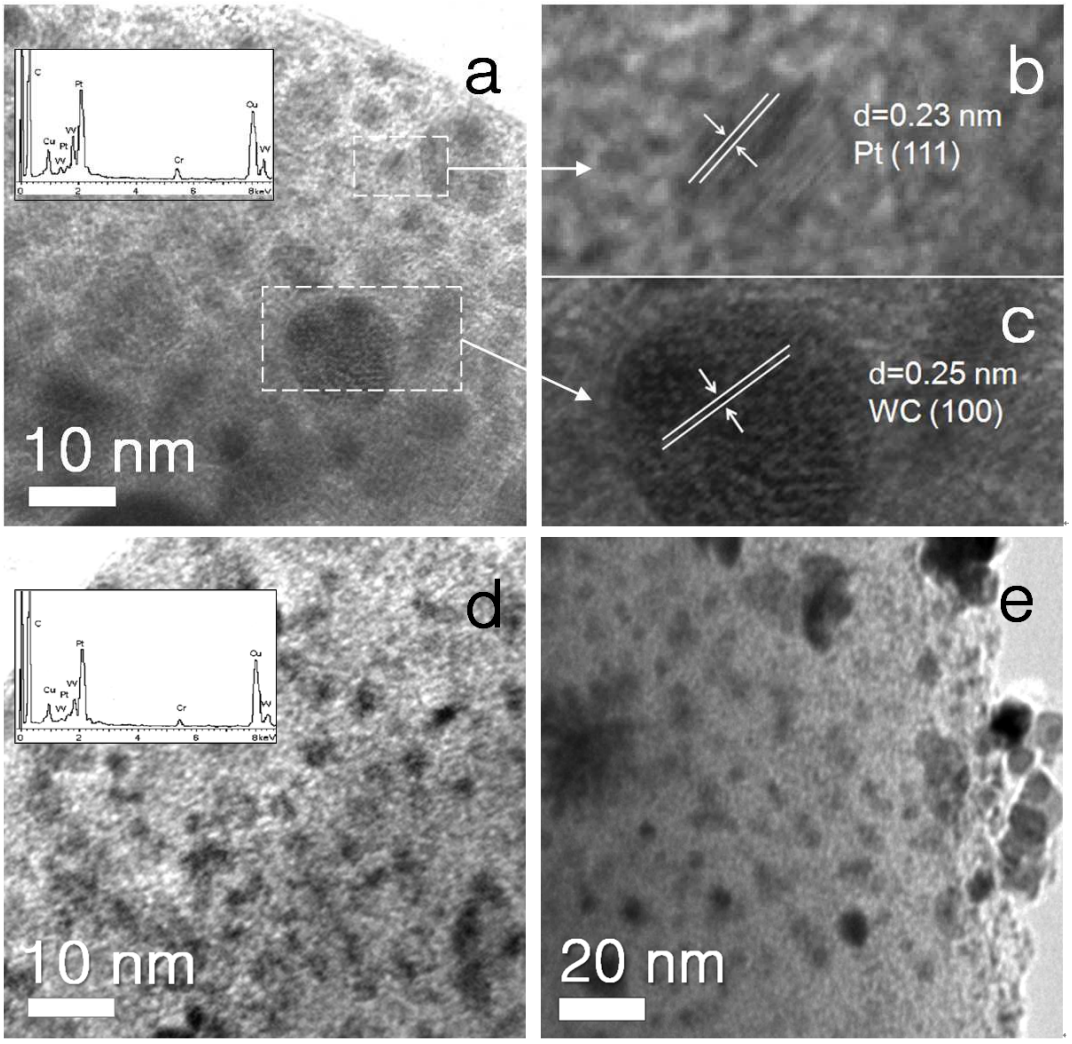

Figure 4

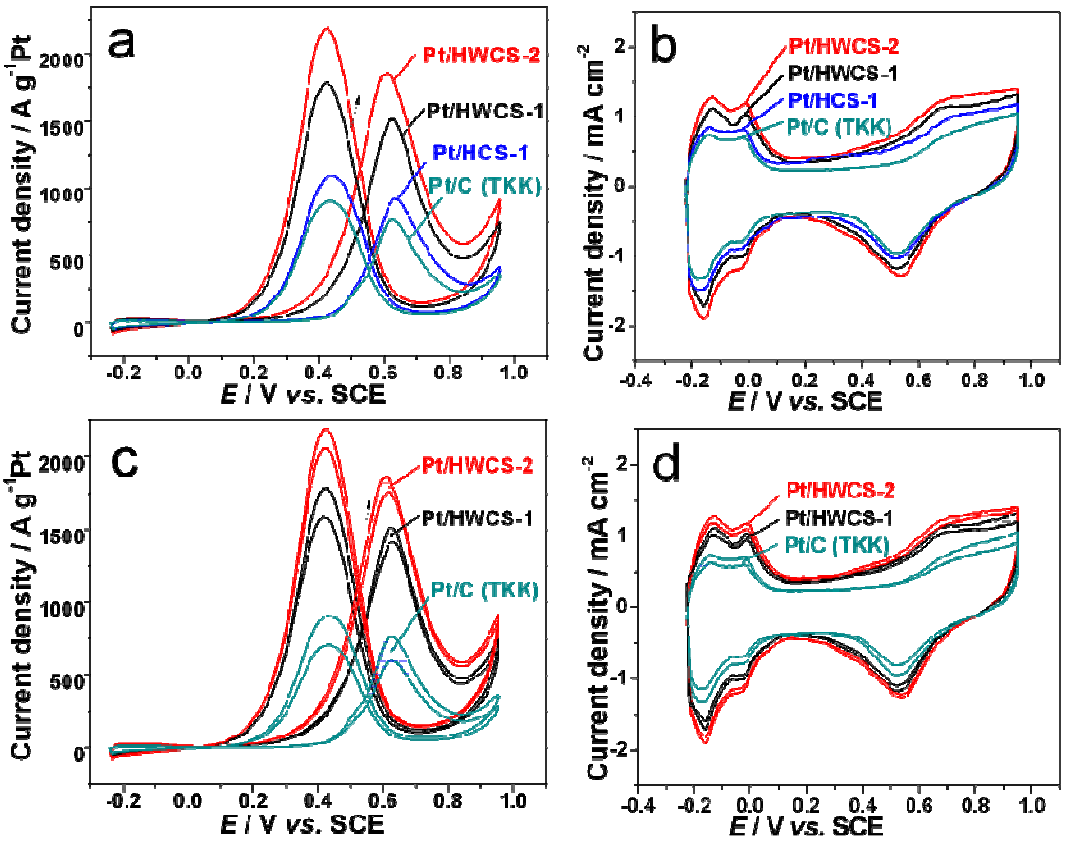

Figure 5